Reversible Multistep and Multielectron Redox Behavior of an Oxo-Centered Trinuclear Ruthenium Complex with a Redox-Active Ligand, $[Ru_3(\mu_3\text{-}O)(\mu\text{-}CH_3CO_2)_6(mbpy^+)_3]^{4+}$ ($mbpy^+$ = *N*-Methyl-4,4′-bipyridinium Ion), and Its Trirhodium and Diruthenium−Rhodium Derivatives

Masaaki Abe,*,†,# Yoichi Sasaki,*,‡ Yasuko Yamada,§ Keiichi Tsukahara,§ Shigenobu Yano,*,§ and Tasuku Ito*,†

Department of Chemistry, Faculty of Science, Tohoku University, Aoba-ku, Aramaki, Sendai 980-77, Japan, Department of Chemistry, Faculty of Science, Hokkaido University, Kita-ku, Sapporo 060, Japan, and Department of Chemistry, Faculty of Science, Nara Women's University, Nara 630, Japan

Received April 26, 1995[⊗]

A series of new oxo-centered triruthenium, trirhodium, and mixed diruthenium−rhodium complexes having three redox-active terminal ligands, *N*-methyl-4,4′-bipyridinium ion ($mbpy^+$), were prepared: $[Ru_3(\mu_3\text{-}O)(\mu\text{-}CH_3CO_2)_6(mbpy^+)_3](PF_6)_3$ (**1**), $[Ru_3(\mu_3\text{-}O)(\mu\text{-}CH_3CO_2)_6(mbpy^+)_3](PF_6)_4$ (**2**), $[Ru_3(\mu_3\text{-}O)(\mu\text{-}C_6H_5CO_2)_6(mbpy^+)_3](PF_6)(ClO_4)_3$ (**3**), $[Ru_2Rh(\mu_3\text{-}O)(\mu\text{-}CH_3CO_2)_6(mbpy^+)_3](ClO_4)_4$ (**4**), and $[Rh_3(\mu_3\text{-}O)(\mu\text{-}CH_3CO_2)_6(mbpy^+)_3](PF_6)_4$ (**5**). Their versatile electrochemical properties were investigated by means of cyclic voltammetry, differential-pulse voltammetry, and controlled-potential absorption spectroscopy. Ru_3 complexes **1** and **2** provide nine-step 11-electron redox waves (involving eight reversible waves) in 0.1 M $(n\text{-}C_4H_9)_4NPF_6$−CH_3CN solution in the range from +2.0 to −3.0 V vs ferrocene/ferrocenium (Fc/Fc^+) couple at 22 °C (M = mol dm^{-3}), consisting of five $Ru_3(\mu_3\text{-}O)$ core-based one-electron processes at +1.62, +0.64, −0.34, −1.75, and −2.76 V and the terminal ligand-based steps at −1.23, −1.37, −1.99, and −2.09 V. The two couples of terminal ligand-based processes, $mbpy^+/mbpy^\bullet$ and $mbpy^\bullet/mbpy^-$, split into two steps in 2:1 current intensity ratio. Complex **3** exhibits similar redox behavior. The Ru_2Rh complex **4** exhibits eight-step 10-electron redox waves (involving six reversible waves), with the core-based redox processes at +1.65, +0.74, −0.72, and −1.88 V, $mbpy^+/mbpy^\bullet$ steps at −1.14, −1.26, and −1.45 V, and $mbpy^\bullet/mbpy^-$ steps at −2.14 V (3e). The Rh_3 complex **5** shows two-step four-electron redox behavior with a core-oxidation at +0.97 V and one-step three $mbpy^+$ reductions at −1.21 V (3e). The splitting of the ligand-based redox waves are caused by the ligand−ligand interactions through an empty $d\pi$−$p\pi$ molecular orbital in the trinuclear $M_3(\mu_3\text{-}O)$ framework.

Introduction

Multiple-electron transfer reactions in transition-metal complexes have received considerable attention in recent years in view of both purely scientific aspect and electrochemical and catalytic applications.[1−6] The design of multielectron redox systems have included approaches to introduction of two or more redox-active metal ions into one structural unit or redox-active ligands into a metal center. Cluster complexes therefore would serve as excellent structural units to such systems.

Oxo-centered carboxylate-bridged trinuclear complexes of the type $[M_3(\mu_3\text{-}O)(\mu\text{-}RCO_2)_6L_3]^{n+}$ (L = neutral monodentate ligand)[7] widely occur in a variety of first-row[8−11] and second- and third-row[12−40] transition-metal ions. Among those, triruthenium analogs exhibit versatile redox properties;[15−40] they serve as reversible multistep and multielectron redox systems. Thus, triruthenium complex $[Ru_3(\mu_3\text{-}O)(\mu\text{-}CH_3CO_2)_6(py)_3]^+$ (py = pyridine) shows four one-electron reversible redox waves at $E_{1/2}$ = +1.67, +0.74, −0.32, and −1.59 V vs Ag/Ag^+ in CH_3CN (0.1 M $[(n\text{-}C_4H_9)_4N]PF_6$) at room temperature (M = mol dm^{-3}).[20] Ruthenium-containing mixed-metal complexes $[Ru^{III}_2M(\mu_3\text{-}O)(\mu\text{-}CH_3CO_2)_6L_3]^{n+}$ (M = Rh^{III} and several first-row transition metal ions; L = pyridine and H_2O; n = 1 and 0)[41,42] also show reversible multistep redox nature. It has been established that the multistep and multielectron redox behavior

† Tohoku University.
‡ Hokkaido University.
§ Nara Women's University.
# Present address: Institute for Molecular Science, Myodaiji, Okazaki 444, Japan.

⊗ Abstract published in *Advance ACS Abstracts*, July 15, 1995.

(1) (a) Rillema, D. P.; Callahan, R. W.; Mack, K. B. *Inorg. Chem.* **1982**, *21*, 2589−2596. (b) Rillema, D. P.; Mack, K. B. *Inorg. Chem.* **1982**, *21*, 3849−3854. (c) Ernst, S. D.; Kaim, W. *Inorg. Chem.* **1989**, *28*, 1520−1528. (d) Fuchs, Y.; Lofters, S.; Dieter, T.; Shi, W.; Morgan, R.; Strekas, T. C.; Gafney, H.; Baker, A. D. *J. Am. Chem. Soc.* **1987**, *109*, 2691−2697. (e) Ernst, S.; Kasack, V.; Kaim, W. *Inorg. Chem.* **1988**, *27*, 1146−1148. (f) Barigelletti, F.; De Cola, L.; Balzani, V.; Hage, R.; Haasnoot, J. G.; Reedjik, J.; Vos, J. G. *Inorg. Chem.* **1989**, *28*, 4344−4350.

(2) Krejčík, M.; Vlček, A. A. *Inorg. Chem.* **1992**, *31*, 2390−2395.

(3) Haga, M.; Bond, A. M. *Inorg. Chem.* **1991**, *30*, 475−480.

(4) (a) Denti, G.; Serroni, S.; Campagna, S.; Juris, A.; Ciano, M.; Balzani, V. *Perspectives in Coordination Chemistry*; Verlag Helvetica Chimica Acta: Basel, 1992; pp 153−164. (b) Serroni, S.; Juris, A.; Campagna, S.; Venturi, M.; Denti, G.; Balzani, V. *J. Am. Chem. Soc.* **1994**, *116*, 9086−9091. (c) Denti, G.; Campagna, S. Serroni, S.; Ciano, M.; Balzani, V. *J. Am. Chem. Soc.* **1992**, *114*, 2944−2950. (d) Campagna, S.; Denti, G.; Sabatino, L.; Serroni, S.; Ciano, M.; Balzani, V. *J. Chem. Soc., Chem. Commun.* **1989**, 1500−1501. (e) Denti, G.; Campagna, S.; Sabatino, L.; Serroni, S.; Ciano, M.; Balzani, V. *Inorg. Chem.* **1990**, *29*, 4750−4758. (f) Campagna, S.; Denti, G.; Serroni, S.; Ciano, M.; Balzani, V. *Inorg. Chem.* **1991**, *30*, 3728−3732. (g) Denti, G.; Campagna, S.; Sabatino, L.; Serroni, S.; Ciano, M.; Balzani, V. *Inorg. Chim. Acta* **1990**, *176*, 175−178. (h) Serroni, Denti, G.; S.; Campagna, S.; Ciano, M.; Balzani, V. *J. Chem. Soc., Chem. Commun.* **1991**, 944−945.

(5) (a) Zanello, P. *Coord. Chem. Rev.* **1988**, *83*, 199−275. (b) Zanello, P. *Coord. Chem. Rev.* **1988**, *87*, 1−54. (c) Astruc, D. *Acc. Chem. Res.* **1986**, *19*, 377−383. (c) Pierpont, C. G.; Buchanan, R. M. *Coord. Chem. Rev.* **1981**, *38*, 45−87. (d) Downs, H. H.; Buchanan, R. M.; Pierpont, C. G. *Inorg. Chem.* **1979**, *18*, 1736−1740.

0020-1669/95/1334-4490$09.00/0

originates from successive electron removal or occupation at $d\pi(Ru)-p\pi(\mu_3\text{-}O)$ molecular orbitals in the trinuclear $Ru_3(\mu_3\text{-}O)$ or $Ru_2M(\mu_3\text{-}O)$ cores.[19a,20,41,42]

It has also been demonstrated that their redox potentials are tunable by synthetic modifications on terminal ligands (L)[22] or bridging carboxylates (RCO_2^-).[26] The triruthenium clusters may be promising as potential electrocatalysts involving multiple electron-transfer processes. It is noteworthy that the triruthenium complexes have been found to be an efficient catalyst to several organic reactions.[38] The triruthenium and the ruthenium-containing mixed-metal complexes may serve as an appropriate cluster unit for the reversible multistep and multielectron redox systems involving as many as 10 or more electrons. Meyer and co-workers reported two extended arrays of triruthenium units by using pyrazine as a bridging ligand: $[\{(py)_2Ru_3(\mu_3\text{-}O)(\mu\text{-}CH_3CO_2)_6\}(\mu\text{-pz})\{Ru_3(\mu_3\text{-}O)(\mu\text{-}CH_3CO_2)_6(py)_2\}](PF_6)_2$[39] and $[(py)_2Ru_3(\mu_3\text{-}O)(\mu\text{-}CH_3CO_2)_6(\mu\text{-pz})]_2[Ru_3(\mu_3\text{-}O)(\mu\text{-}CH_3CO_2)_6(CO)]$[40] (pz = pyrazine). These compounds show reversible redox waves involving 8 or more than 10 electrons in CH_3CN, respectively. However, no further works to construct these extended oligomers have appeared.[43]

Our approach to the multielectron redox systems is to introduce redox-active monodentate ligands to the redox-active trinuclear cluster units. We chose *N*-methyl-4,4′-bipyridinium ion ($mbpy^+$) as a redox-active ligand,[44,45] which undergoes successive two one-electron reversible reductions in non-aqueous media to produce $mbpy^•$ and $mbpy^-$ species, respectively.[46]

In this paper, we describe versatile electrochemical behavior

(6) (a) Wheeler, B. L.; Nagasubramanian, G.; Bard, A. J.; Schechtman, L. A.; Dininny, D. R.; Kenny, M. E. *J. Am. Chem. Soc.* **1984**, *106*, 7404−7410. (b) Nevin, W. A.; Hempstead, M. R.; Liu, W.; Leznoff, C. C.; Lever, A. B. P. *Inorg. Chem.* **1987**, *26*, 570−577. (c) Kobayashi, N.; Lam, H.; Nevin, W. A.; Janda, P.; Leznoff, C. C.; Lever, A. B. P. *Inorg. Chem.* **1990**, *29*, 3415−3425.

(7) Cannon R. D.; White, R. P. *Prog. Inorg. Chem.* **1988**, *36*, 195−298.

(8) "V_3" complexes: (a) Cotton, F. A.; Lewis, G. E.; Mott, G. N. *Inorg. Chem.* **1982**, *21*, 3127−3130. (b) Cotton, F. A.; Lewis, G, E.; Mott, G. N. *Inorg. Chem.* **1982**, *21*, 3316−3321. (c) Cotton, F. A.; Extine, M. W.; Falvello, L. R.; Lewis, D. B.; Lewis, G. E.; Murillo, C. A.; Schwotzer, W.; Tomas, M.; Troup, J. M. *Inorg. Chem.* **1986**, *25*, 3505−3512.

(9) "Cr_3" complexes: (a) Cotton, F. A.; Wang, W. *Inorg. Chem.* **1982**, *21*, 2675−2678. (b) Gonzalez-Vergara, E.; Hegenauer, J.; Saltman, P. *Inorg. Chim. Acta* **1982**, *66*, 115−118. (c) Kato, H.; Nakata, K.; Nagasawa, A.; Yamaguchi, T.; Sasaki, Y.; Ito, T. *Bull. Chem. Soc. Jpn.* **1991**, *64*, 3463−3465. (d) Anson, C. E.; Chai-Sa'ard, N.; Bourke, J. P.; Cannon, R. D.; Jayasooriya, U. A.; Powell, A. K. *Inorg. Chem.* **1993**, *32*, 1502−1507.

(10) "Mn_3" complexes: (a) Baikie, A. R. E.; Hursthouse, M. B.; New, D. B.; Thornton, P. *J. Chem. Soc., Chem. Commun.* **1978**, 62−63. (b) Vincent, J. B.; Chang, H.-R.; Folting, K.; Huffman, J. C.; Christou, G.; Hendrickson, D. N. *J. Am. Chem. Soc.* **1987**, *109*, 5703−5711. (c) Nakano, M.; Sorai, M.; Vincent, J. B.; Christou, G.; Jang, H. G.; Hendrickson, D. N. *Inorg. Chem.* **1989**, *28*, 4608−4614. (d) Jang, H. G.; Vincent, J. B.; Nakano, M.; Huffmann, J. C.; Christou, G.; Sorai, M.; Wittebort, R. J.; Hendrickson, D. N. *J. Am. Chem. Soc.* **1989**, *111*, 7778−7784.

(11) "Fe_3" complexes: (a) Blake, A. B.; Fraser, L. R. *J. Chem. Soc., Dalton Trans.* **1975**, 193−197. (b) Woehler, S. E.; Wittebort, R. J.; Oh, S. M.; Hendrickson, D. N.; Inniss, D.; Strouse, C. E. *J. Am. Chem. Soc.* **1986**, *108*, 2938−2946. (c) Woehler, S. E.;Wittebort, R. J.; Oh, S. M.; Wilson, S. R.; Kambara, T.; Hendrickson, D. N.; Inniss, D.; Strouse, C. E. *J. Am. Chem. Soc.* **1987**, *109*, 1063−1072. (d) Oh, S. M.; Hendrickson, D. N.; Woehler, S. E.; Wittebort, R. J.; Innis, D.; Strouse, C. E. *J. Am. Chem. Soc.* **1987**, *109*, 1073−1090. (e) Nakata, K.; Nagasawa, A.; Sasaki, Y.; Ito, T. *Chem. Lett.* **1989**, 753−756. (f) McCusker, J. K.; Jang, H. G.; Zvagulis, M.; Ley, W.; Drickamer, H. G.; Hendrickson, D. N. *Inorg. Chem.* **1991**, *30*, 1985−1990.

(12) (a) Glowiak, T.; Kubiak, M.; Szymańska-Buzar, T.; Jezouska-Trzebiatowska, B. *Acta Crystallogr., Sect. B: Struct. Crystallogr. Cryst. Chem.* **1977**, *B33*, 3106−3109. (b) Baranovskii, I. B.; Mazo, G. Y.; Dikareva, L. M. *Russ. J. Inorg. Chem.* **1971**, *16*, 1388−1389.

(13) Takahashi, K.; Umakoshi, K.; Kikuchi, A.; Sasaki, Y. *Z. Naturforsch., Sect. B*, in press.

(14) Brown, D. B.; Robin, M. B.; McIntyre, J. D. E.; Peck, W. F. *Inorg. Chem.* **1970**, *9*, 2315−2320.

(15) Uemura, S.; Spencer, A.; Wilkinson, G. *J. Chem. Soc., Dalton Trans.* **1973**, 2565−2571.

(16) (a) Cotton, F. A.; Wilkinson, G. *Advanced Inorganic Chemistry*; 5th ed.; Wiley: New York, 1988; p 896. (b) Mehrotra, R. C.; Bohra, R. *Metal Carboxylates*; Academic Press: London, 1983. (c) Wilkinson, G. *Comprehensive Coordination Chemistry*, 1st ed.; Pergamon Press: Oxford, England, 1987; pp 427−429.

(17) Spencer, A.; Wilkinson, G. *J. Chem. Soc., Dalton Trans.* **1972**, 1570−1577.

(18) Spencer, A.; Wilkinson, G. *J. Chem. Soc., Dalton Trans.* **1974**, 786−792.

(19) (a) Cotton, F. A.; Norman, J. G. Jr. *Inorg. Chim. Acta* **1972**, *6*, 411−419. (b) Cotton, F. A.; Norman, J. G. Jr.; Spencer, A.; Wilkinson, G. *Chem. Commun.* **1971**, 967−968.

(20) Baumann, J. A.; Salmon, D. J.; Wilson, S. T.; Meyer, T. J.; Hatfield, W. E. *Inorg. Chem.* **1978**, *17*, 3342−3350.

(21) Walsh, J. L.; Baumann, J. A.; Meyer, T. J. *Inorg. Chem.* **1980**, *19*, 2145−2151.

(22) Toma, H. E.; Cunha, C. J.; Cipriano, C. *Inorg. Chim. Acta* **1988**, *154*, 63−66.

(23) Toma, H. E.; Cunha, C. J. *Can. J. Chem.* **1989**, *67*, 1632−1635.

(24) Abe, M.; Sasaki, Y.; Nagasawa, A.; Ito, T. *Bull. Chem. Soc. Jpn.* **1992**, *65*, 1411−1414.

(25) Kobayashi, H.; Uryu, N.; Tokiwa, A. Yamaguchi, T.; Sasaki, Y.; Ito, T. *Bull. Chem. Soc. Jpn.* **1992**, *65*, 198−202.

(26) Abe, M.; Sasaki, Y.; Yamaguchi, T.; Ito, T. *Bull. Chem. Soc. Jpn.* **1992**, *65*, 1585−1590.

(27) Almog, O.; Bino, A.; Garfinkel-Shweky, D. *Inorg. Chim. Acta* **1993**, *213*, 99−102.

(28) Powell, G.; Richens, D. T.; Powell, A. K. *Inorg. Chim. Acta* **1993**, *213*, 147−155.

(29) Sasaki, Y.; Nagasawa, A.; Tokiwa-Yamamoto, A.; Ito, T. *Inorg. Chim. Acta* **1993**, *212*, 175−182.

(30) Toma, H. E.; Alexiou, D. P. *Electrochimica Acta* **1993**, *38*, 975−980.

(31) Toma, H. E.; Matsumoto, F. M.; Cipriano, C. *J. Electroanal. Chem.* **1993**, *346*, 261−270.

(32) Toma, H. E.; Olive, M. A. L. *Polyhedron* **1994**, *13*, 2647−2652.

(33) Cosnier, S.; Deronzier, A.; Llobet, A. *J. Electroanal. Chem.* **1990**, *280*, 213.

(34) Akashi, D.; Kido, H.; Sasaki, Y.; Ito, T. *Chem Lett.* **1992**, 143−146.

(35) (a) Johnson, M. K.; Powell, D. B.; Cannon, R. D. *Spectrochim. Acta* **1981**, *37A*, 995−1006. (b) Johnson, M. K.; Cannon, R. D.; Powell, D. B. *Spectrochim. Acta* **1982**, *38A*, 307−315.

(36) Imamura, T.; Sumiyoshi, T.; Takahashi, K.; Sasaki, Y. *J. Phys. Chem.* **1993**, *97*, 7786−7791.

(37) Ohto, A.; Tokiwa-Yamamoto, A.; Abe, M.; Ito, T.; Sasaki, Y.; Umakoshi, K.; Cannon, R. D. *Chem. Lett.* **1995**, 97−98.

(38) (a) Davis, S.; Drago, R. S. *J. Chem. Soc., Chem. Commun.* **1990**, 250−251. (b) Davis, S.; Drago, R. S. *Inorg. Chem.* **1988**, *27*, 4759−4760. (c) Bilgrien, C.; Davis. S.; Drago, R. S. *J. Am. Chem. Soc.* **1987**, *109*, 3786−3787. (d) Ito, S.; Aihara, K.; Matsumoto, M. *Tetrahedron Lett.* **1983**, *24*, 5249−5252. (e) Carlsen, P. H. J.; Katsuki, T.; Martin, V. S.; Sharpless, K. B. *J. Org. Chem.* **1981**, *46*, 3936−3938. (f) Fouda, S. A.; Rempel, G. L. *Inorg. Chem.* **1979**, *18*, 1−8. (g) Milner, D. J.; Whelan, R. *J. Organomet. Chem.* **1978**, *152*, 193−195. (h) Fouda, S. A.; Hui, B. C. Y.; Rempel, G. L. *Inorg. Chem.* **1978**, *17*, 3213−3220. (i) Sasson, Y.; Rempell, G. L. *Tetrahedron Lett.* **1974**, *47*, 4133−4136. (j) Sasson, Y.; Rempel, G. L. *Can. J. Chem.* **1974**, *52*, 3825−3827. (k) Mitchell, R. W.; Spencer, A.; Wilkinson, G. *J. Chem. Soc., Dalton Trans.* **1973**, 846−854. (l) Legzding, P.; Mitchell, R. W.; Rempel, G. L.; Ruddick, J. D.; Wilkinson, G. *J. Chem. Soc. A* **1970**, 3322−3326.

(39) (a) Baumann, J. A.; Salmon, D. J.; Wilson, S. T.; Meyer, T. J. *Inorg. Chem.* **1979**, *18*, 2472−2479. (b) Wilson, S. T.; Bondurant, R. F.; Meyer, T. J.; Salmon, D. J. *J. Am. Chem. Soc.* **1975**, *97*, 2285−2287.

(40) Baumann, J. A.; Wilson, S. T.; Salmon, D. J.; Hood, P. L.; Meyer, T. J. *J. Am. Chem. Soc.* **1979**, *101*, 2916−2920.

(41) Sasaki, Y.; Tokiwa, A.; Ito, T. *J. Am. Chem. Soc.* **1987**, *109*, 6341−6347.

(42) (a) $[Ru^{III}_2M(\mu_3\text{-}O)(\mu\text{-}CH_3CO_2)_6(py)_3]\cdot py$ (M = Ni^{II} and Co^{II}): Ohto, A; Sasaki, Y; Ito, T. *Inorg. Chem.* **1994**, *33*, 1245−1246. (b) $[Ru^{III}_2M(\mu_3\text{-}O)(\mu\text{-}CH_3CO_2)_6(py)_3]^{n+}$ (M = Co^{II}, n = 0 and Co^{III}, n = 1): Don, T-Y.; Lee, H.-S.; Lee, T.-Y.; Hsieh, C-F. *J. Chin. Chem. Soc.* **1992**, *39*, 393−399. (c) $[Ru^{III}_2Cr^{III}(\mu_3\text{-}O)(\mu\text{-}CH_3CO_2)_6(py)_3]^+$: Sasaki, Y.; Yoshida, Y.; Ohto, A.; Tokiwa, A.; Ito, T.; Kobayashi, H.; Uryu, N.; Mogi, I. *Chem. Lett.* **1993**, 69−72.

(43) The pyrazine-bridged trimer of triruthenium unit $[(L)_2Ru_3(\mu_3\text{-}O)(\mu\text{-}CH_3CO_2)_6(\mu\text{-pz})]_2[Ru_3(\mu_3\text{-}O)(\mu\text{-}CH_3CO_2)_6(CO)]$ (L = pyridine derivatives) and the tetramer $[(py)_2Ru_3(\mu_3\text{-}O)(\mu\text{-}CH_3CO_2)_6(\mu\text{-pz})\}_3\{Ru_3(\mu_3\text{-}O)(\mu\text{-}CH_3CO_2)_6\}](PF_6)_4$ have recently been prepared in our laboratories. Unpublished results.

(44) Leopold, K. R.; Haim, A. *Inorg. Chem.* **1978**, *17*, 1753−1757.

Chart 1

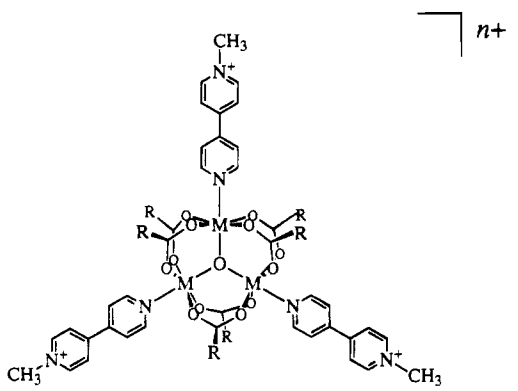

$[Ru^{II}Ru^{III}_2(\mu_3\text{-}O)(\mu\text{-}CH_3CO_2)_6(mbpy^+)_3](PF_6)_3$ **1**

$[Ru^{III}_3(\mu_3\text{-}O)(\mu\text{-}CH_3CO_2)_6(mbpy^+)_3](PF_6)_4$ **2**

$[Ru^{III}_3(\mu_3\text{-}O)(\mu\text{-}C_6H_5CO_2)_6(mbpy^+)_3](PF_6)(ClO_4)_3$ **3**

$[Ru^{III}_2Rh^{III}(\mu_3\text{-}O)(\mu\text{-}CH_3CO_2)_6(mbpy^+)_3](ClO_4)_4$ **4**

$[Rh^{III}_3(\mu_3\text{-}O)(\mu\text{-}CH_3CO_2)_6(mbpy^+)_3](PF_6)_4$ **5**

$mbpy^+ =$ 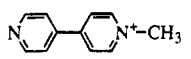

of the triruthenium complexes having three $mbpy^+$ ligands, $[Ru_3(\mu_3\text{-}O)(\mu\text{-}CH_3CO_2)_6(mbpy^+)_3](PF_6)_3$ (**1**), $[Ru_3(\mu_3\text{-}O)(\mu\text{-}CH_3CO_2)_6(mbpy^+)_3](PF_6)_4$ (**2**), and $[Ru_3(\mu_3\text{-}O)(\mu\text{-}C_6H_5CO_2)_6(mbpy^+)_3](PF_6)(ClO_4)_3$ (**3**). Mixed-metal Ru_2Rh and Rh_3 analogs $[Ru_2Rh(\mu_3\text{-}O)(\mu\text{-}CH_3CO_2)_6(mbpy^+)_3](ClO_4)_4$ (**4**) and $[Rh_3(\mu_3\text{-}O)(\mu\text{-}CH_3CO_2)_6(mbpy^+)_3](PF_6)_4$ (**5**) are also prepared (see Chart 1). Cyclic and differential-pulse voltammetric studies confirmed that the Ru_3 and the Ru_2Rh complexes exhibited multistep redox processes, in which 11 and 10 electrons were involved, respectively. These redox waves are unambiguously assigned either trinuclear metal-centered or terminal ligand-centered processes on the basis of cyclic- and differential-pulse voltammetry together with controlled-potential absorption spectroscopy. It was found that the $mbpy^+/mbpy^•$ process split into two and three steps in the Ru_3 and the Ru_2Rh complexes, respectively. In contrast, the Rh_3 analog shows no splitting in the corresponding process. Interactions between the terminal ligands in **1**–**5** are also discussed.

Experimental Section

1. Preparation of Precursor Oxo-Centered Trinuclear Complexes and the Ligand. a. $[Ru^{III}_3(\mu_3\text{-}O)(\mu\text{-}C_6H_5CO_2)_6(C_2H_5OH)_3]PF_6$. Previously we reported a benzoate-bridged triruthenium complex $[Ru_3(\mu_3\text{-}O)(\mu\text{-}C_6H_5CO_2)_6(py)_3]PF_6$.[26] In this study, the C_2H_5OH derivative was isolated as a precursor to complex **3**. To a hot suspension of NaOH (1.00 g, 0.025 mmol) and benzoic acid (10.0 g, 82.0 mmol) in C_2H_5OH (20 cm^3) was added a C_2H_5OH solution (25 cm^3) of $RuCl_3•nH_2O$ (1.00 g). The solution was refluxed for an hour, during which the color changed from red-brown to dark green. The resulting solution was cooled to room temperature and filtered. Dark green filtrate was evaporated to ca. 20 cm^3 and was treated with column chromatography (Sephadex LH-20 resin). A blue green band was eluted with C_2H_5OH. The eluent was evaporated to ca. 20 cm^3, and NH_4PF_6 (0.20 g, 1.23 mmol) was added. Addition of *n*-hexane (50 cm^3) produced black crystals of $[Ru_3(\mu_3\text{-}O)(\mu\text{-}C_6H_5CO_2)_6(C_2H_5OH)_3]PF_6•3H_2O$ in 18% yield (380 mg). Anal. Calcd for $[Ru_3(\mu_3\text{-}O)(\mu\text{-}C_6H_5CO_2)_6(C_2H_5OH)_3]PF_6•3H_2O$: C, 40.77; H, 3.73%. Found: C, 40.66; H, 3.65%. FAB MS, m/z = 1139 ($[Ru_3O(C_6H_5CO_2)_6(C_2H_5OH)_2(H_2O)]^+$). Electronic spectrum ($C_2H_5OH$), λ_{max}/nm (ϵ/M^{-1} cm^{-1}): 680 (2600), 610 (2600), 300_{sh} (20700), 270_{sh} (25300), 230 (81700). ^1H NMR (CD_3CN) δ 9.91 (12H, Ph-1,5-H), 8.13 (6H, Ph-3-H), 7.88 (12H, Ph-2,4-H), 3.54 (6H, $-CH_2-$), 1.11 (9H, CH_3).

b. Other Materials. The ligand $[mbpy^+]PF_6$ was prepared according to the reported methods with slight modifications.[44] (μ_3-Oxo)hexakis(μ-acetato)tris(methanolruthenium(III)) acetate, $[Ru^{III}_3(\mu_3\text{-}O)(\mu\text{-}CH_3CO_2)_6(CH_3OH)_3](CH_3CO_2)$,[20] ($\mu_3$-oxo)hexakis($\mu$-acetato)tris(aquarhodium(III)) perchlorate, $[Rh^{III}_3(\mu_3\text{-}O)(\mu\text{-}CH_3CO_2)_6(H_2O)_3]ClO_4$,[41] ($\mu_3$-oxo)hexakis($\mu$-acetato)bis(aquaruthenium(III))aquarhodium(III) perchlorate, $[Ru^{III}_2Rh^{III}(\mu_3\text{-}O)(\mu\text{-}CH_3CO_2)_6(H_2O)_3]ClO_4$,[41] and their pyridine analogs were synthesized according to the reported methods.

2. Preparations of the Complexes Having $mbpy^+$ Ligands. a. $[Ru^{II}Ru^{III}_2(\mu_3\text{-}O)(\mu\text{-}CH_3CO_2)_6(mbpy^+)_3](PF_6)_3$ (1). To a CH_3OH solution (50 cm^3) of $[Ru^{III}_3(\mu_3\text{-}O)(\mu\text{-}CH_3CO_2)_6(CH_3OH)_3](CH_3CO_2)$[20] (420 mg, 0.51 mmol) was added $[mbpy^+]PF_6$ (510 mg, 1.61 mmol). Refluxing of the mixture for an hour gave deep purple microcrystals of $[Ru^{II}Ru^{III}_2(\mu_3\text{-}O)(\mu\text{-}CH_3CO_2)_6(mbpy^+)_3](PF_6)_3•2H_2O$ in 52% yield (440 mg). Anal. Calcd for $[Ru_3(\mu_3\text{-}O)(\mu\text{-}CH_3CO_2)_6(mbpy^+)_3](PF_6)_3•2H_2O$: 32.59; H, 3.35; N, 5.07. Found: C, 32.48; H, 3.23; N, 4.97. FAB MS, m/z = 1622 ($[Ru_3O(CH_3CO_2)_6(mbpy^+)_3](PF_6)_3^+$). IR (1800–1400 cm^{-1} region, KBr pellet, cm^{-1}) 1430 s (ν_{sym}(COO)), 1650 s, 1610 m, 1540 m, 1500 m.

b. $[Ru^{III}_3(\mu_3\text{-}O)(\mu\text{-}CH_3CO_2)_6(mbpy^+)_3](PF_6)_4$ (2). To a CH_3OH solution (20 cm^3) of $[Ru^{II}Ru^{III}_2(\mu_3\text{-}O)(\mu\text{-}CH_3CO_2)_6(mbpy^+)_3](PF_6)_3•2H_2O$ (70 mg, 0.042 mmol) was added 10% of Br_2/CH_3OH solution dropwise until the color changed from deep purple to green. An addition of NH_4PF_6 (50 mg, 0.31 mmol) with stirring afforded green precipitates, which were collected and washed with CH_3OH and diethyl ether. Recrystallization of the crude product from acetone/*n*-hexane (1/1 v/v) at 0 °C gave $[Ru^{III}_3(\mu_3\text{-}O)(\mu\text{-}CH_3CO_2)_6(mbpy^+)_3](PF_6)_4•H_2O$ in 78% yield (60 mg). The sample for electrochemical measurements was obtained by column chromatographic purification (Sephadex LH-20 resin, CH_3CN). Green main fraction was collected, evaporated to dryness, and the residue was recrystallized from CH_3CN/diethyl ether (1/1 v/v). Anal. Calcd for $[Ru_3(\mu_3\text{-}O)(\mu\text{-}CH_3CO_2)_6(mbpy^+)_3](PF_6)_4•H_2O$: C, 30.28; H, 3.00; N, 4.71. Found: C, 30.38; H, 3.11; N, 4.67. FAB MS, m/z = 1622 ($[Ru_3O(CH_3CO_2)_6(mbpy^+)_3(PF_6)_3]^+$). IR (1800–1400 cm^{-1} region, cm^{-1}): 1430 s (ν_{sym}(COO)), 1650 s, 1620 m, 1580 w, 1550 m, 1535 m, 1500 m.

c. $[Ru^{III}_3(\mu_3\text{-}O)(\mu\text{-}C_6H_5CO_2)_6(mbpy^+)_3](PF_6)(ClO_4)_3$ (3). To a C_2H_5OH solution (30 cm^3) of $[Ru^{III}_3(\mu_3\text{-}O)(\mu\text{-}C_6H_5CO_2)_6(C_2H_5OH)_3]PF_6•3H_2O$ (100 mg, 0.075 mmol) was added $[mbpy^+]PF_6$ (100 mg, 0.32 mmol), and the solution was refluxed for 30 min, during which the color changed from blue-green to dark green, and then green solid products formed. These were collected and washed with hot C_2H_5OH and then diethyl ether (160 mg). A CH_3CN solution (2 cm^3) of crude products was subjected to column chromatography (Sephadex LH-20 resin, C_2H_5OH). A green main fraction was collected (ca. 10 cm^3), $NaClO_4$ (0.2 g) and water (10 cm^3) were added, and the mixture was allowed to stand for 3 days at 0 °C. Microcrystalline solids formed were recrystallized from hot CH_3OH to give $[Ru^{III}_3(\mu_3\text{-}O)(\mu\text{-}C_6H_5CO_2)_6(mbpy^+)_3](PF_6)(ClO_4)_3•6H_2O$ in 62% yield (91 mg). Anal. Calcd for $[Ru_3(\mu_3\text{-}O)(\mu\text{-}C_6H_5CO_2)_6(mbpy^+)_3](PF_6)(ClO_4)_3•6H_2O$: C, 42.67; H, 3.59; N, 3.98. Found: C, 42.80; H, 3.61; N, 3.94. FAB MS, m/z = 1857 ($[Ru_3O(C_6H_5CO_2)_6(mbpy^+)_3•(ClO_4)_3]^+$). IR (1800–1400 cm^{-1} region, cm^{-1}): 1425 s (ν_{sym}(COO)), 1640 m, 1620 m, 1580 w, 1540 m, 1530 m, 1500 m.

d. $[Ru^{III}_2Rh^{III}(\mu_3\text{-}O)(\mu\text{-}CH_3CO_2)_6(mbpy^+)_3](ClO_4)_4$ (4). To an aqueous solution (20 cm^3) of $[Ru^{III}_2Rh^{III}(\mu_3\text{-}O)(\mu\text{-}CH_3CO_2)_6(H_2O)_3]ClO_4•5NaClO_4$[41] (100 mg, 0.069 mmol) was added a CH_3OH solution (20 cm^3) of $[mbpy^+]PF_6$ (280 mg, 0.89 mmol), and the mixture was heated under reflux for 1 h. Green products obtained by evaporation of the reaction mixture were purified by column chromatography (Sephadex LH-20 resin with acetone as an eluent). The green main fraction was evaporated to ca. 10 cm^3, and diethyl ether (20 cm^3) was

(45) Examples for compounds having $mbpy^+$: (a) Tsukahara, K.; Wilkins, R. G. *Inorg. Chem.* **1989**, *28*, 1605–1607. (b) Chen, P.; Curry, M.; Meyer, T. J. *Inorg. Chem.* **1989**, *28*, 2271–2280. (c) Sullivan, B. P.; Abruna, H.; Finklea, H. O.; Salmon, D. J.; Nagle, J. K.; Meyer, T. J.; Sprintschnick, H. *Chem. Phys. Lett.* **1978**, *58*, 389–393.

(46) In this text, one-electron and two-electron reduced species of $mbpy^+$ are abbreviated as $mbpy^•$ and $mbpy^-$, respectively. Redox potentials of $[mbpy^+]PF_6$ ($E_{1/2}$ in V vs Fc/Fc^+ in 0.1 M $[(n\text{-}C_4H_9)_4N]PF_6$–$CH_3CN$ at 22 ± 1 °C. In parentheses are given ΔE_p in mV): $E_{1/2}$ = −1.33 (60) [$mbpy^+/mbpy^•$], −2.02 (60) [$mbpy^•/mbpy^-$].

added to give green precipitates in 87% yield (130 mg). Microcrystals were obtained with recrystallization from hot CH_3OH. Anal. Calcd for $[Ru_2Rh(\mu_3\text{-}O)(\mu\text{-}CH_3CO_2)_6(mbpy^+)_3](ClO_4)_4{\cdot}NaClO_4{\cdot}2H_2O$: C, 30.96; H, 3.18; N, 4.82. Found: C, 31.10; H, 3.11; N, 4.80. FAB MS, *m/z* = 1019 ($[Ru_2RhO(CH_3CO_2)_6(mbpy^+)_2]^+$). IR (1800−1400 cm^{-1} region, cm^{-1}): 1590 s (ν_{asym}(COO)), 1420 s (ν_{sym}(COO)), 1640 m, 1560 m, 1490 m.

e. $[Rh^{III}_3(\mu_3\text{-}O)(\mu\text{-}CH_3CO_2)_6(mbpy^+)_3](PF_6)_4$ (5). $[Rh^{III}_3(\mu_3\text{-}O)(\mu\text{-}CH_3CO_2)_6(H_2O)_3]ClO_4$[41] (70 mg, 0.084 mmol) and $[mbpy^+]PF_6$ (140 mg, 0.44 mmol) were dissolved in CH_3OH (20 cm^3), and the mixture was refluxed for 1 h, affording yellow microcrystalline precipitates in 48% yield (73 mg). Anal. Calcd for $[Rh_3(\mu_3\text{-}O)(\mu\text{-}CH_3CO_2)_6(mbpy^+)_3](PF_6)_4{\cdot}3H_2O$: C, 29.59; H, 3.15; N, 4.60. Found: C, 29.49; H, 3.34; N, 4.61. FAB MS, *m/z* = 1626 ($[Rh_3O(CH_3CO_2)_6(mbpy^+)_3](PF_6)_3^+$). IR (1800−1400 cm^{-1} region, cm^{-1}): 1620 s (ν_{asym}(COO)), 1425 s (ν_{sym}(COO)), 1550 w, 1530 w, 1500 w.

Caution! Although the perchlorate salts reported in this study were not found to be explosive, the materials should be handled with extreme care in small quantities.

3. Materials. CH_3CN used in electrochemical measurements was distilled twice over P_4O_{10} and then once over CaH_2 under a nitrogen atmosphere before use. Tetra-*n*-butylammonium hexafluorophosphate $[(n\text{-}C_4H_9)_4N]PF_6$ was prepared by mixing aqueous solutions of $[(n\text{-}C_4H_9)_4N]Br$ and of NH_4PF_6, and then was recrystallized three times from hot ethylacetate/benzene and dried in vacuo at 140 °C for more than 12 h. $RuCl_3{\cdot}nH_2O$, $RhCl_3{\cdot}3H_2O$ (Wako Pure Chemicals), and other reagents were used as received.

4. Measurements. Electronic absorption spectra were recorded on a Hitachi 330 or 340 spectrophotometer. ^1H NMR spectra were obtained on a JEOL GSX-270 FT NMR spectrometer at 270 MHz. Infrared absorption spectra were recorded with KBr pellets on a Jasco IR-810 spectrophotometer. Mass spectra were measured with a JEOL JMS-HX 110 mass spectrometer with 3-nitrobenzyl alcohol as a matrix.

Cyclic voltammetry (CV) and differential-pulse voltammetry (DPV) were carried out by using a YANACO P-1100 polarographic analyzer with a WATANABE WX 1100 X-Y recorder. A three-electrode cell consisting of a glassy carbon working electrode, a platinum wire counter electrode, and an Ag/Ag^+ ($[AgClO_4]$ = 0.01 M in CH_3CN) reference electrode was used. CV was performed at scan rates of 5 to 500 mV s^{-1}. The half-wave potentials $E_{1/2} = (E_{pc} + E_{pa})/2$, where E_{pc} and E_{pa} are the cathodic and anodic peak potential, respectively, are given at a scan rate of 100 mV s^{-1}. Under these experimental conditions, the one-electron reversible wave of ferrocene (1 mM) was detected at $E_{1/2}$ = +0.09 V vs Ag/Ag^+ with ΔE_p ($= E_{pa} - E_{pc}$) = 60 mV. DPV was performed at scan rates of 5−20 mV s^{-1} with pulse height of 5 mV. Coulometry was carried out with a thin-layer cell.[47] Controlled potential absorption spectra were obtained with an optically transparent thin-layer electrode (OTTLE) cell (an optical path length, 0.5 mm) by using a gold mesh working electrode in conjunction with the Hitachi 330 spectrophotometer. All electrochemical and spectroelectrochemical measurements were carried out under a nitrogen atmosphere.

Results

1. Preparation of the New Complexes. Reactions of trinuclear complexes having three coordinated solvent molecules $[M^{III}_3(\mu_3\text{-}O)(\mu\text{-}CH_3CO_2)_6(S)_3]^+$ (M_3 = Ru_3, Rh_3, and Ru_2Rh; S = CH_3OH or H_2O) and $[Ru^{III}_3(\mu_3\text{-}O)(\mu\text{-}C_6H_5CO_2)_6(C_2H_5OH)_3]^+$ with excess $[mbpy^+]PF_6$ in CH_3OH (or CH_3OH/H_2O) at refluxing temperature produce the corresponding $mbpy^+$ derivatives. These synthetic procedures are analogous to those for the pyridine complexes $[M_3(\mu_3\text{-}O)(\mu\text{-}CH_3CO_2)_6(py)_3]^+$ (M_3 = Ru_3,[20] Ru_2Rh,[41] and Rh_3[41]) and $[Ru^{III}_3(\mu_3\text{-}O)(\mu\text{-}C_6H_5CO_2)_6(py)_3]^+$.[26] For the acetate-bridged Ru_3 complex, $Ru^{II}Ru^{III}_2$ complex **1** rather than Ru^{III}_3 complex **2** precipitates under the present synthetic conditions. The divalent state in complex **1** is considered to be delocalized over the three Ru ions as previously mentioned for other $Ru^{II}Ru^{III}_2$ complexes.[20] Oxidation states of isolated Ru_3 complexes may depend on the nature of terminal ligands as well as bridging carboxylates.[48] Ru^{III}_3 complex **2** is obtained by bromine oxidation of $Ru^{II}Ru^{III}_2$ complex **1**. The symmetrical carboxylate stretching vibrations, ν_{sym}(COO), of Ru_3 complexes **1**, **2**, and **3** in IR spectra appear in the range 1420−1430 cm^{-1} with strong absorptions. However, the asymmetrical ones ν_{asym}(COO) are unclear due to a significant overlap with those from the coordinated $mbpy^+$ ligands. In contrast, both stretches are detectable in Rh_2Rh complex **4** (ν_{asym}(COO) = 1590 and ν_{sym}(COO) = 1420 cm^{-1}) and Rh_3 complex **5** (ν_{asym}(COO) = 1620 and ν_{sym}(COO) = 1425 cm^{-1}) with strong vibrations. The different band shape of ν_{asym}(COO) has been seen in the aqua and pyridine complexes of these three Ru_3, Rh_3, and Ru_2Rh cores, and was discussed in terms of symmetry lowering of the Ru_3 complexes.[37] Differences between ν_{asym}(COO) and ν_{sym}(COO) (170 cm^{-1} for **4** and 195 cm^{-1} for **5**) indicate a bridging mode of the acetate ions.[16b,50] All acetate-bridged $mbpy^+$ compounds are highly soluble in CH_3CN, $(CH_3)_2CO$, and water. This is in marked contrast to high solubility of the py and the aqua complexes only in organic solvents and water, respectively. The present complexes are fairly stable in solutions as evidenced by absorption and ^1H NMR spectroscopy.

2. ^1H NMR Spectroscopy. ^1H NMR chemical shifts for complexes **1**−**5** in CD_3CN at 25 °C and their assignments are listed in Table 1 along with those of the free $mbpy^+$ ligand. Complexes **1** ($Ru^{II}Ru^{III}_2$), **4** ($Ru^{III}_2Rh^{III}$), and **5** (Rh^{III}_3) are essentially diamagnetic.[20,41] Signals of aromatic and methyl protons of coordinated $mbpy^+$ ligands of complexes **1**, **4**, and **5** appear in the ranges δ 9.49−8.13 and δ 4.45−4.39 in CD_3CN, respectively. They are slightly downfield shifted as compared with those of a free $mbpy^+$ ligand (δ 8.84−7.79 for aromatic ring protons and δ 4.32 for CH_3 in CD_3CN). Acetate methyl resonances are observed in the range δ 2.03−2.56. In the Ru_2Rh complex **4**, two kinds resonances with 2:1 integrated intensity ratios are observed, reflecting the symmetry lowering of the trinuclear core.[41] Resonances of complexes **2** and **3** (Ru^{III}_3) are paramagnetically shifted, but they are rather sharp.[20] As compared with the free ligand, aromatic and methyl protons of coordinated $mbpy^+$ ligands in **2** and **3** show upfield and downfield shift, respectively. Acetate methyl resonance of **2** exhibits downfield shift as compared with the diamagnetic $Ru^{II}Ru^{III}_2$ analog **1**. The trend in chemical shifts on going from $Ru^{II}Ru^{III}_2$ to Ru^{III}_3 complexes is in fair agreement with that observed in $[Ru_3(\mu_3\text{-}O)(\mu\text{-}CH_3CO_2)_6(py)_3]^{n+}$ (n = 0 and 1).[20]

3. Absorption Spectroscopy. Absorption spectral data of the new complexes in CH_3CN and H_2O are collected in Table 2, in which each absorption spectrum is classified into three bands (bands I−III). The present complexes exhibit distinctive spectral patterns. Ru_3 complexes **1**−**3** and Ru_2Rh complex **4**

(47) Unoura, K.; Iwase, A.; Ogino, H. *J. Electroanal. Chem.* **1990**, *295*, 385−392.

(48) The spontaneous one-electron reduction also took place for the tris(4-cyanopyridine) and tris(pyrazine) complexes,[49] while not for the tris(pyridine) complex and $mbpy^+$ derivative of the Ru_3 μ-benzoate complex **3**.

(49) Hashimoto, M.; Hishikawa, M.; Abe, M.; Sasaki, Y.; Ito, T. Unpublished results.

(50) Nakamoto, K. *Infrared and Raman Spectra of Inorganic and Coordination Compounds*, 4th ed.; John Wiley & Sons: New York, 1986.

(51) In order to determine the multistep redox waves of Ru_3 and Ru_2Rh complexes with $mbpy^+$ ligands, redox potentials of the known pyridine complexes were remeasured under the present condition ($E_{1/2}$ in V vs Fc/Fc^+ in 0.1 M $[(n\text{-}C_4H_9)_4N]PF_6$−$CH_3CN$ at 22 ± 1 °C. In parentheses are given ΔE_p values in mV. Scan rate, 100 mV s^{-1}). $[Ru_3(\mu_3\text{-}O)(\mu\text{-}CH_3CO_2)_6(py)_3]PF_6$: $E_{1/2}$ = +1.56 (100), +0.59 (70), −0.47 (60), −1.74 (70), and E_{pc} = −2.45 V.; $[Ru_3(\mu_3\text{-}O)(\mu\text{-}C_6H_5CO_2)_6(py)_3]PF_6$: $E_{1/2}$ = +1.49 (100), +0.62 (70), −0.35 (60), and −1.63 (60) V.; $[Ru_2Rh(\mu_3\text{-}O)(\mu\text{-}CH_3CO_2)_6(py)_3]ClO_4$: $E_{1/2}$ = +1.68 (70), +0.79 (60), −0.77 (60) V, and E_{pc} = −1.80 V.

Table 1. ^{1}H NMR Data for the Ligand and the New Complexes[a]

complex	aromatic (mbpy$^+$)				CH_3	
					mbpy$^+$	acetate
[mbpy$^+$]PF_6	8.84 (2H, d)	8.71 (2H, d)	8.30 (2H, d)	7.79 (2H, d)	4.32 (3H, s)	
$[Ru_3(\mu_3\text{-}O)(\mu\text{-}CH_3CO_2)_6(mbpy^+)_3](PF_6)_3$ (**1**)	9.49 (6H, d)	8.82 (6H, d)	8.53 (6H, d)	8.25 (6H, d)	4.39 (9H, s)	2.03 (18H, s)
$[Ru_3(\mu_3\text{-}O)(\mu\text{-}CH_3CO_2)_6(mbpy^+)_3](PF_6)_4$ (**2**)	8.45 (6H, d)	7.67 (6H, s)	5.85 (6H, s)	0.75 (6H, s)	4.11 (9H, s)	5.39 (18H, s)
$[Ru_3(\mu_3\text{-}O)(\mu\text{-}C_6H_5CO_2)_6(mbpy^+)_3](PF_6)(ClO_4)_3$ (**3**)	8.49 (6H, d)	7.78 (6H, d)	6.15 (6H, s)	1.67 (6H, s)	4.12 (9H, s)	
	(phenyl ring: 9.57 (12H, d, Ph-2,6-H), 7.89 (6H, t, Ph-4-H), 7.78 (12H, t, Ph-3,5-H))					
$[Ru_2Rh(\mu_3\text{-}O)(\mu\text{-}CH_3CO_2)_6(mbpy^+)_3](ClO_4)_4$ (**4**)	8.99 (4H, d)[b]	8.88 (4H, d)[b]	8.53 (4H, d)[b]	8.45 (4H, d)[b]	4.45 (6H, s)[b]	2.56 (12H, s)[d]
	9.22 (2H, d)[c]	8.85 (2H, d)[c]	8.45 (2H, d)[c]	8.23 (2H, d)[c]	4.42 (3H, s)[c]	2.07 (6H, s)[e]
$[Rh_3(\mu_3\text{-}O)(\mu\text{-}CH_3CO_2)_6(mbpy^+)_3](PF_6)_4$ (**5**)	9.01 (6H, d)	8.82 (6H, d)	8.42 (6H, d)	8.13 (6H, d)	4.39 (9H, s)	2.24 (18H, s)

[a] In CD_3CN at 25 °C. Chemical shifts are referenced to TMS. [b] Coordinated to Ru. [c] Coordinated to Rh. [d] Bridging Ru···Rh. [e] Bridging Ru···Ru.

Table 2. Absorption Spectral Data for the New Complexes in CH_3CN and Water[a]

complex	solvent	λ_{max}/nm (ϵ/M^{-1} cm^{-1})		
		band I[b]	band II[c]	band III[d]
$[Ru_3(\mu_3\text{-}O)(\mu\text{-}CH_3CO_2)_6(mbpy^+)_3](PF_6)_3$ (**1**)	CH_3CN	950 (25000)	570 (18600), 350sh (9800)	260 (94800)
	water	910 (20900)	502 (16300)	260 (90200)
$[Ru_3(\mu_3\text{-}O)(\mu\text{-}CH_3CO_2)_6(mbpy^+)_3](PF_6)_4$ (**2**)	CH_3CN	700 (8300), 620sh (5800)	395 (12900)	255 (63900)
	water	700 (8300), 620sh (5800)	380sh (11400), 330sh (14700)	252 (61000)
$[Ru_3(\mu_3\text{-}O)(\mu\text{-}C_6H_5CO_2)_6(mbpy^+)_3](PF_6)(ClO_4)_3$ (**3**)	CH_3CN	718 (8700)	392 (16600)	270sh (77100)
				235 (114600)[e]
$[Ru_2Rh(\mu_3\text{-}O)(\mu\text{-}CH_3CO_2)_6(mbpy^+)_3](ClO_4)_4$ (**4**)	CH_3CN	596 (5200)	408 (11000), 364 (10900)	255 (63900)
	water	597 (5200)	408sh (7100), 360sh (10600)	250 (54800)
$[Rh_3(\mu_3\text{-}O)(\mu\text{-}CH_3CO_2)_6(mbpy^+)_3](PF_6)_4$ (**5**)	CH_3CN		388 (6400)	252 (62900)
	water		370sh (10100)	250 (62200)

[a] Measured at 25 °C. sh = shoulder. [b] Transitions between molecular orbitals arising from dπ(metal)−pπ(μ_3-O) interactions within the $M_3(\mu_3$-O) core. [c] Charge-transfer transitions from dπ−pπ orbitals of the $M_3(\mu_3$-O) core to π^* orbitals of the mbpy$^+$ ligands. [d] $\pi-\pi^*$ transitions in mbpy$^+$ ligands. [e] $\pi-\pi^*$ transitions in benzoate phenyl rings.

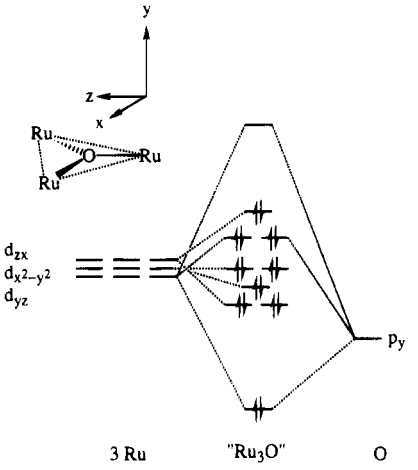

Figure 1. Qualitative molecular orbital diagram for oxo-centered triruthenium unit. A total of 18 electrons are shown in the diagram, which corresponds to $Ru^{II}Ru^{III}_2$ oxidation state.

display two absorption bands in a visible region, while Rh_3 complex **5** exhibits no strong band. These visible absorption features are explained in terms of qualitative molecular orbital diagram for the $Ru_3(\mu_3$-O) cluster π system in D_{3h} symmetry proposed by Cotton and Norman[19a] and by Meyer and co-workers,[20] as shown in Figure 1. The molecular orbitals arising from the interactions between ruthenium dπ orbitals (d_{zx}, d_{xy}, d_{yz}) and a central oxide p_z orbital with an sp^2 hybridization give one bonding, one antibonding, and eight essentially nonbonding orbitals. The $Ru^{II}Ru^{III}_2$ complex, as shown in Figure 1, has 18 electrons in one bonding and eight nonbonding orbitals (16 from three Ru ions and two from a central oxide ion). The analogous MO-type interactions are also proposed for both Rh_3 and mixed-metal Ru_2Rh complexes.[41]

Broad absorption band centered at 700 nm (ϵ = 8300 M^{-1} cm^{-1}) with a shoulder (around 620 nm) for Ru^{III}_3 complex **2** in CH_3CN is assigned to transitions from occupied nonbonding orbitals to a vacant antibonding orbital (band I). These transitions are also observed for other Ru^{III}_3 analogs in the similar wavelength region.[20,22,23,26] An absorption centered at 395 nm (ϵ = 12 900 M^{-1} cm^{-1}) is attributed to charge-transfer transitions from dπ−pπ molecular orbitals in the $Ru_3(\mu_3$-O) core to π^* orbitals of the coordinated mbpy$^+$ ligands (band II). This assignment is supported by a significant shift of the band maxima depending on the terminal ligands.[20,22] In $Ru^{II}Ru^{III}_2$ complex **1**, both absorption bands are shifted toward a longer wavelength region compared with those observed in Ru^{III}_3 complex **2**. This trend is in agreement with that found for the pyridine analogs $[Ru_3(\mu_3\text{-}O)(\mu\text{-}CH_3CO_2)_6(py)_3]^{n+}$ (n = 0, 1).[20] An absorption band around 260 nm can be assigned to $\pi-\pi^*$ transitions of terminal mbpy$^+$ ligands (band III). $Ru^{III}_2Rh^{III}$ complex **4** also shows three types of absorption bands.[41] The Rh^{III}_3 complex, in which all dπ−pπ orbitals are filled with 20 electrons, shows no intense absorptions over 400 nm.[14,41]

The absorption spectra of the mbpy$^+$ complexes of Ru_3, Ru_2Rh, and Rh_3 in organic solvents are appreciably different from those in water. Solvent effects on absorption spectra of oxo-centered trinuclear complexes in both organic and aqueous solutions have not been reported previously. A charge-transfer band (band II) in Ru^{III}_3 complex **2** in CH_3CN (λ_{max} = 395 nm) shifts to shorter wavelength in water with distinctive two shoulders (around 380 and 330 nm), while transitions between the dπ−pπ MO's of the trinuclear core (band I) and the $\pi-\pi^*$ transitions of coordinated mbpy$^+$ ligands (band III) remain almost unchanged in both solvents. The substantial solvent effect seen only in the charge-transfer band is also observed in the Ru_2Rh and the Rh_3 analogs (Table 2).

4. Electrochemical Behavior. Figures 2−4 show cyclic and differential-pulse voltammograms of complexes **2**, **4**, and **5** in a 0.1 M $[(n\text{-}C_4H_9)_4N]PF_6$−$CH_3CN$ solution at room temperature, respectively. The process numbering classified by the nature of the redox waves are also included. Their $E_{1/2}$ values are tabulated in Table 3.

a. $[Ru_3(\mu_3\text{-}O)(\mu\text{-}CH_3CO_2)_6(mbpy^+)_3]^{4+}$. As shown in

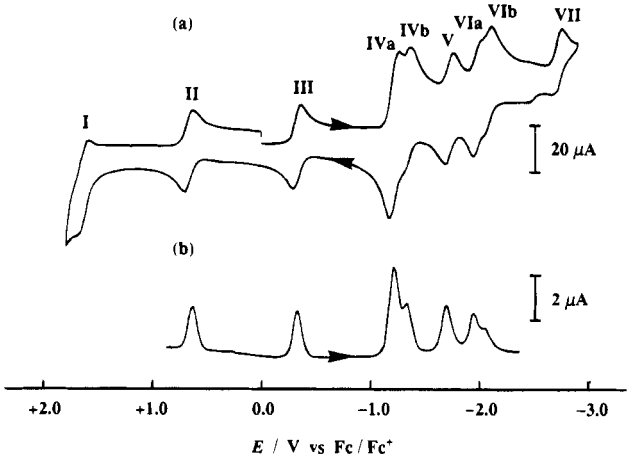

Figure 2. Cyclic voltammogram (a) and differential-pulse voltammogram (b) of $[Ru_3(\mu_3\text{-}O)(\mu\text{-}CH_3CO_2)_6(mbpy^+)_3]^{4+}$ in a 0.1 M $[(n\text{-}C_4H_9)_4N]PF_6$–$CH_3CN$ solution. Scan rate = 100 mV s^{-1} for cyclic voltammetry and 5 mV s^{-1} for differential-pulse voltammetry, respectively.

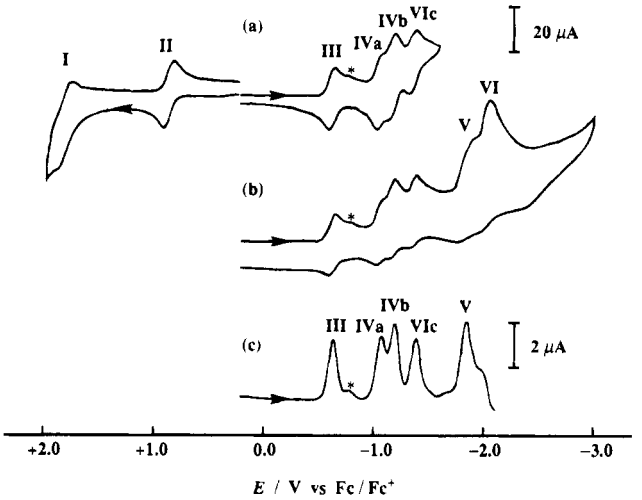

Figure 3. Cyclic voltammograms (a and b) and differential-pulse voltammogram (c) of $[Ru_2Rh(\mu_3\text{-}O)(\mu\text{-}CH_3CO_2)_6(mbpy^+)_3]^{4+}$ in a 0.1 M $[(n\text{-}C_4H_9)_4N]PF_6$–$CH_3CN$ solution. Scan rate = 100 mV s^{-1} for cyclic voltammetry and 20 mV s^{-1} for differential-pulse voltammetry. Asterisks are due to an impurity.

Figure 2, complex **2** exhibits essentially reversible multistep redox processes. Eight reversible steps labeled I to VIb and one irreversible step labeled VII are obtained in 0.1 M $[(n\text{-}C_4H_9)_4N]PF_6$–$CH_3CN$ in the range from +2.0 to −3.0 V vs Fc/Fc^+, which involves a total of 11 electrons (*vide supra*). Complex **1** gives the same CV and DPV as complex **2**. Comparison of the redox potentials with those of $[Ru_3(\mu_3\text{-}O)(\mu\text{-}CH_3CO_2)_6(py)]PF_6$[51] enables us to assign reversible waves I, II, III, and V ($E_{1/2}$ = +1.62, +0.64 , −0.34, and −1.75 V, respectively) and an irreversible wave VII (E_{pc} = −2.76 V) to $Ru_3(\mu_3\text{-}O)$ trinuclear core-based processes of $Ru^{III}Ru^{IV}_2/Ru^{III}_2Ru^{IV}/.../Ru^{II}_3$. A coulometric measurement at −0.2 V established that process III is of one-electron nature ($n = 0.9 \pm 0.1$). The other trinuclear core-based waves are also concluded to be one-electron processes as judged from the current intensities.

Processes IVa, IVb and VIa, VIb are terminal ligand-based. It is interesting to note that the $mbpy^+/mbpy^\bullet$ process splits into two steps with 2:1 current intensity ratio (IVa and IVb), which are clearly detectable as two peaks in DPV at −1.23 and −1.37

(52) When the potential is scanned to −3.0 V, ill-defined irreversible waves are detected in CV at E_{pc} = −1.35, −1.69, −2.00, and −2.62 V.

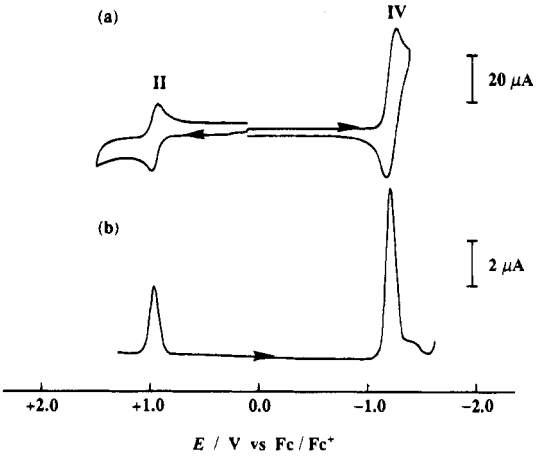

Figure 4. Cyclic voltammogram (a) and differential-pulse voltammogram (b) of $[Rh_3(\mu_3\text{-}O)(\mu\text{-}CH_3CO_2)_6(mbpy^+)_3]^{4+}$ in a 0.1 M $[(n\text{-}C_4H_9)_4N]PF_6$–$CH_3CN$ solution. Scan rate = 100 mV s^{-1} for cyclic voltammetry and 20 mV s^{-1} for differential-pulse voltammetry.

V. Splitting feature is also seen in the $mbpy^\bullet/mbpy^-$ process (−1.99 and −2.09 V for processes VIa and VIb, respectively). The redox processes of Ru_3 complex **2** are summarized as follows:

$$[Ru^{III}Ru^{IV}_2(\mu_3\text{-}O)(\mu\text{-}CH_3CO_2)_6(mbpy^+)_3]^{6+}$$

$$+e^- \uparrow\downarrow -e^- \quad \text{(I)}$$

$$[Ru^{III}_2Ru^{IV}(\mu_3\text{-}O)(\mu\text{-}CH_3CO_2)_6(mbpy^+)_3]^{5+}$$

$$+e^- \uparrow\downarrow -e^- \quad \text{(II)}$$

$$[Ru^{III}_3(\mu_3\text{-}O)(\mu\text{-}CH_3CO_2)_6(mbpy^+)_3]^{4+}$$

$$+e^- \uparrow\downarrow -e^- \quad \text{(III)}$$

$$[Ru^{II}Ru^{III}_2(\mu_3\text{-}O)(\mu\text{-}CH_3CO_2)_6(mbpy^+)_3]^{3+}$$

$$+2e^- \uparrow\downarrow -2e^- \quad \text{(IVa)}$$

$$[Ru^{II}Ru^{III}_2(\mu_3\text{-}O)(\mu\text{-}CH_3CO_2)_6(mbpy^+)(mbpy^\bullet)_2]^{+}$$

$$+e^- \uparrow\downarrow -e^- \quad \text{(IVb)}$$

$$[Ru^{II}Ru^{III}_2(\mu_3\text{-}O)(\mu\text{-}CH_3CO_2)_6(mbpy^\bullet)_3]^{0}$$

$$+e^- \uparrow\downarrow -e^- \quad \text{(V)}$$

$$[Ru^{II}_2Ru^{III}(\mu_3\text{-}O)(\mu\text{-}CH_3CO_2)_6(mbpy^\bullet)_3]^{-}$$

$$+2e^- \uparrow\downarrow -2e^- \quad \text{(VIa)}$$

$$[Ru^{II}_2Ru^{III}(\mu_3\text{-}O)(\mu\text{-}CH_3CO_2)_6(mbpy^\bullet)(mbpy^-)_2]^{3-}$$

$$+e^- \uparrow\downarrow -e^- \quad \text{(VIb)}$$

$$[Ru^{II}_2Ru^{III}(\mu_3\text{-}O(\mu\text{-}CH_3CO_2)_6(mbpy^-)_3]^{4-}$$

$$+e^- \uparrow\downarrow -e^- \quad \text{(VII)}$$

$$[Ru^{II}_3(\mu\text{-}CH_3CO_2)_6(mbpy^-)_3]^{3-} + O^{2-}$$

A substantial effect of the complex charge on the core-based redox potentials should be noted. The complex species involved in the electrode process have highly positive and negative charges (+6 to −4), and this leads to a positive shift in the potentials for processes I, II, and III and a negative shift for process VII in the case of **2** relative to those for the Ru_3–pyridine complex.[51]

The irreversible process in the most negative region ($Ru^{II}_2Ru^{III}/Ru^{II}_3$) has been previously claimed to be accompanied by a loss

of central μ_3-oxide ion.[15,23] We assume that the similar μ_3-oxide loss also takes place in complex **2** (process VII).

b. $[Ru_3(\mu_3\text{-}O)(\mu\text{-}C_6H_5CO_2)_6(mbpy^+)_3]^{4+}$. The benzoate-bridged Ru_3 complex **3** also exhibits multistep redox behavior arising from both the $Ru_3(\mu_3\text{-}O)$ framework and the terminal ligands. The stronger electron withdrawing property of benzoate ions leads to the positive shifts in the core-based redox potential for complex **3** relative to those for acetate-bridged complex **2** (by 70−190 mV). The same trend has been found in pyridine complexes $[Ru_3(\mu_3\text{-}O)(\mu\text{-}CH_3CO_2)_6(py)_3]PF_6$ and $[Ru_3(\mu_3\text{-}O)(\mu\text{-}C_6H_5CO_2)_6(py)_3]PF_6$.[26] Ligand-based processes are observed at $E_p = -1.25$ and -1.36 V for $mbpy^+/mbpy^\bullet$ (IVa and IVb) and -2.05 and -2.10 V for $mbpy^\bullet/mbpy^-$ (VIa and IVb) in DPV. Splitting of ligand-based redox waves (110 mV for $mbpy^+/mbpy^\bullet$ and 50 mV for $mbpy^\bullet/mbpy^-$) is comparable to the case for the acetato complex **2**. The effects of bridging carboxylate on the terminal ligand reduction potentials and the extent of their splittings seem to be small.

c. $[Ru_2Rh(\mu_3\text{-}O)(\mu\text{-}CH_3CO_2)_6(mbpy^+)_3]^{4+}$. This complex shows six reversible one-electron redox waves and two irreversible waves in the range from +2.0 to −3.0 V as shown in Figure 3. Reversible processes labeled I, II, and III ($E_{1/2} = +1.65$, +0.74, and −0.72 V, respectively, Figure 3a) and an irreversible process V ($E_p = -1.88$ V, Figure 3b) are assignable to redox in the $Ru_2Rh(\mu_3\text{-}O)$ moiety.[41,51] The first oxidation wave (process II) should certainly correspond to $Ru^{III}_2Rh^{III}/Ru^{III}Ru^{IV}Rh^{III}$ redox couple. The second oxidation (process I) is due to either one-electron oxidation of the second Ru or the Rh site. A group of the splitting process labeled IVa−IVc is ligand-based ($E_p = -1.14$, -1.26, and -1.45 V in DPV, Figure 3c). In contrast, one-step reductions are observed for the $mbpy^\bullet/mbpy^-$ process at $E_{pc} = -2.14$ V (3e) in CV (process VI). The redox processes of Ru_2Rh complex **4** can be summarized as follows:

$$[Ru^{IV}_2Rh^{III}(\mu_3\text{-}O)(\mu\text{-}CH_3CO_2)_6(mbpy^+)_3]^{6+}$$
$$(\text{or } [Ru^{III}Ru^{IV}Rh^{IV}(\mu_3\text{-}O)(\mu\text{-}CH_3CO_2)_6(mbpy^+)_3]^{6+})$$
$$+e^- \uparrow\downarrow -e^- \quad \text{(I)}$$
$$[Ru^{III}Ru^{IV}Rh^{III}(\mu_3\text{-}O)(\mu\text{-}CH_3CO_2)_6(mbpy^+)_3]^{5+}$$
$$+e^- \uparrow\downarrow -e^- \quad \text{(II)}$$
$$[Ru^{III}_2Rh^{III}(\mu_3\text{-}O)(\mu\text{-}CH_3CO_2)_6(mbpy^+)_3]^{4+}$$
$$+e^- \uparrow\downarrow -e^- \quad \text{(III)}$$
$$[Ru^{II}Ru^{III}Rh^{III}(\mu_3\text{-}O)(\mu\text{-}CH_3CO_2)_6(mbpy^+)_3]^{3+}$$
$$+e^- \uparrow\downarrow -e^- \quad \text{(IVa)}$$
$$[Ru^{II}Ru^{III}Rh^{III}(\mu_3\text{-}O)(\mu\text{-}CH_3CO_2)_6\ (mbpy^+)_2(mbpy^\bullet)]^{2+}$$
$$+e^- \uparrow\downarrow -e^- \quad \text{(IVb)}$$
$$[Ru^{II}Ru^{III}Rh^{III}(\mu_3\text{-}O)(\mu\text{-}CH_3CO_2)_6(mbpy^+)_2(mbpy^\bullet)_2]^{+}$$
$$+e^- \uparrow\downarrow -e^- \quad \text{(IVc)}$$
$$[Ru^{II}Ru^{III}Rh^{III}(\mu_3\text{-}O)(\mu\text{-}CH_3CO_2)_6(mbpy^\bullet)_3]^{0}$$
$$+e^- \uparrow\downarrow -e^- \quad \text{(V)}$$
$$[Ru^{II}_2Rh^{III}(\mu_3\text{-}O)(\mu\text{-}CH_3CO_2)_6(mbpy^\bullet)_3]^{-}$$
$$+3e^- \uparrow\downarrow -3e^- \quad \text{(VI)}$$
$$[Ru^{II}_2Rh^{III}(\mu_3\text{-}O)(\mu\text{-}CH_3CO_2)_6(mbpy^-)_3]^{4-}$$

d. $[Rh_3(\mu_3\text{-}O)(\mu\text{-}CH_3CO_2)_6(mbpy^+)_3]^{4+}$. The complex displays a reversible one-electron redox couple labeled II at $E_{1/2} = +0.97$ V and a one-step quasi-reversible process of $mbpy^+/mbpy^\bullet$ labeled IV at $E_p = -1.21$ V in the range +2.0 to −1.3 V (Figure 4).[52] The process II corresponds to $Rh^{III}_3/Rh^{III}_2Rh^{IV}$. One-electron nature of the Rh_3 core-based process has been previously established for analogs with other terminal ligands.[13,41] Process IV involves three electrons, judging from relative current intensity ratio between the two couples. The redox processes of Rh_3 complex **5** can be summarized as follows:

$$[Rh^{III}_2Rh^{IV}(\mu_3\text{-}O)(\mu\text{-}CH_3CO_2)_6(mbpy^+)_3]^{5+}$$
$$+e^- \uparrow\downarrow -e^- \quad \text{(II)}$$
$$[Ru^{III}_3(\mu_3\text{-}O)(\mu\text{-}CH_3CO_2)_6(mbpy^+)_3]^{4+}$$
$$+3e^- \uparrow\downarrow -3e^- \quad \text{(IV)}$$
$$[Ru^{III}_3(\mu_3\text{-}O)(\mu\text{-}CH_3CO_2)_6(mbpy^\bullet)_3]^{-}$$

5. Controlled-Potential Absorption Spectroscopy of the Triruthenium Complex. In order to identify the multistep redox waves, controlled-potential absorption spectra were measured by using a gold mesh working electrode with an optically transparent thin-layered electrode (OTTLE) cell. Absorption spectra at controlled potentials were reported for $[Ru_3(\mu_3\text{-}O)(\mu\text{-}CH_3CO_2)_6(isonic)_3]$ (isonic = isonicotineamide)[23] and $[Ru_3(\mu_3\text{-}O)(\mu\text{-}CH_3CO_2)_6(py)_2(dmso)]$ (dmso = dimethyl sulfoxide).[30] Absorption spectra of Ru_3 complex **2** in 0.1 M $[(n\text{-}C_4H_9)_4N]PF_6$−$CH_3CN$ at given potentials are displayed in Figure 5. Absorption spectra of electrochemically generated reduced species could be taken only up to process IVb (Figure 2). When the potential was set at more negative potential (beyond process V), the absorption intensity in a visible region decreased during the electrolysis and the spectroelectrochemical study on the highly reduced species of **2** was impossible. It is demonstrated that one-electron oxidized species $[Ru^{III}_2Ru^{IV}(\mu_3\text{-}O)(\mu\text{-}CH_3CO_2)_6(mbpy^+)_3]^{5+}$ (at +0.9 V) gives absorption maxima at 790, 576, and 322 nm (Figure 5a). This spectrum is compared with that of $[Ru^{III}_2Ru^{IV}(\mu_3\text{-}O)(\mu\text{-}CH_3CO_2)_6(py)_3]^{2+}$, which shows absorption maxima at 775, 575, and 313 nm in CH_2Cl_2.[20] One-electron reduced species $[Ru^{II}Ru^{III}_2(\mu_3\text{-}O)(\mu\text{-}CH_3CO_2)_6(mbpy^+)_3]^{3+}$ (at −1.0 V) gives absorption maxima at 950 and 570 nm (Figure 5c), which are close to those of **1**. When the potential is applied to −1.5 V (a potential between processes IVb and V), three absorption bands are observed at 992 nm ($\epsilon = 9600\ M^{-1}\ cm^{-1}$), 514 nm ($\epsilon = 22\,600\ M^{-1}\ cm^{-1}$), and 370 nm ($\epsilon = 41\,700\ M^{-1}\ cm^{-1}$) (Figure 5d). Since free $mbpy^\bullet$ shows absorptions at 369 and 535 nm (at −1.7 V) under the same conditions, the band centered at 370 nm is assigned to a $\pi-\pi^*$ transition of three coordinated $mbpy^\bullet$ ligands and an absorption at 514 nm are assigned to overlap of two types of transitions, charge-transfer transitions ($Ru_3(\mu_3\text{-}O)$ core to $mbpy^\bullet$ ligands) and another $\pi-\pi^*$ transition in $mbpy^\bullet$ ligands. This spectrum clearly indicates that processes IVa and IVb are ligand-centered.

One-electron reduced Ru_2Rh complex $[Ru^{II}Ru^{III}Rh^{III}(\mu_3\text{-}O)(\mu\text{-}CH_3CO_2)_6(mbpy^+)_3]^{5+}$ (at −0.9 V) shows three bands at 1277, 667, and 410 nm. Measurements of absorption spectra at potentials in which one or more $mbpy^+$ ligands are reduced (< −1.1 V) were failed due to the instability of those species.

Discussion

Multistep and Multielectron Redox Behavior. Several types of compounds which exhibit multistep and multielectron redox behavior have been extensively studied. The typical

Table 3. Redox Potentials of $[M_3(\mu_3\text{-}O)(\mu\text{-}CH_3CO_2)_6(mbpy^+)_3]^{4+}$ (M_3 = Ru_3 (**2**), Ru_2Rh (**4**), and Rh_3 (**5**)) and $[Ru_3(\mu_3\text{-}O)(\mu\text{-}C_6H_5CO_2)_6(mbpy^+)_3]^{4+}$ (**3**) in 0.1 M $[(n\text{-}C_4H_9)_4N]PF_6$-$CH_3CN$[a]

assignment	numbering	$E_{1/2}$[b]/V vs Fc/Fc^+ (ΔE_p[c]), ne[d]			
		2	**3**	**4**	**5**
(III,IV,IV)/(III,III,IV)	**I**	+1.62 (110), 1e		+1.65 (90), 1e	
(III,III,IV)/(III,III,III)	**II**	+0.64 (70), 1e	+0.73 (80), 1e	+0.74 (60), 1e	+0.97 (50), 1e
(III,III,III)/(II,III,III)	**III**	−0.34 (50), 1e	−0.15 (70), 1e	−0.72 (50), 1e	
$mbpy^+/mbpy^•$	**IVa**	−1.23,[e] 2e	−1.25,[e] 2e	−1.14,[e] 1e	−1.21 (100),[g] 3e
	IVb	−1.37,[e] 1e	−1.36[e], 1e	−1.26,[e] 1e	
	IVc			−1.45,[e] 1e	
(II,III,III)/(II,II,III)	**V**	−1.75 (60), 1e	−1.68 (90), 1e	−1.88,[f] 1e	
$mbpy^•/mbpy^-$	**VIa**	−1.99,[e] 2e	−2.05,[e] 2e	−2.14,[f] 3e	
	VIb	−2.09,[e] 1e	−2.10,[e] 1e		
(II,II,III)/(II,II,II)	**VII**	−2.76,[f] 1e	−2.58,[f] 1e		

[a] Measured at 22 ± 1 °C at a scan rate of 100 mV s^{-1} by using a glassy carbon working electrode, a platinum coil counter electrode, and an Ag/Ag^+ ($[AgClO_4]$ = 0.01 mM in CH_3CN) reference electrode. [complex] = 1 mM. All potentials are reported vs Fc/Fc^+ couple. [b] $E_{1/2} = (E_{pa} + E_{pc})/2$, where E_{pa} and E_{pc} are anodic and cathodic peak potentials, respectively. [c] $\Delta E_p = E_{pa} - E_{pc}$. [d] ne = number of electrons exchanged. [e] Peak potential in DPV. [f] E_{pc} for the irreversible process. [g] Quasireversible process.

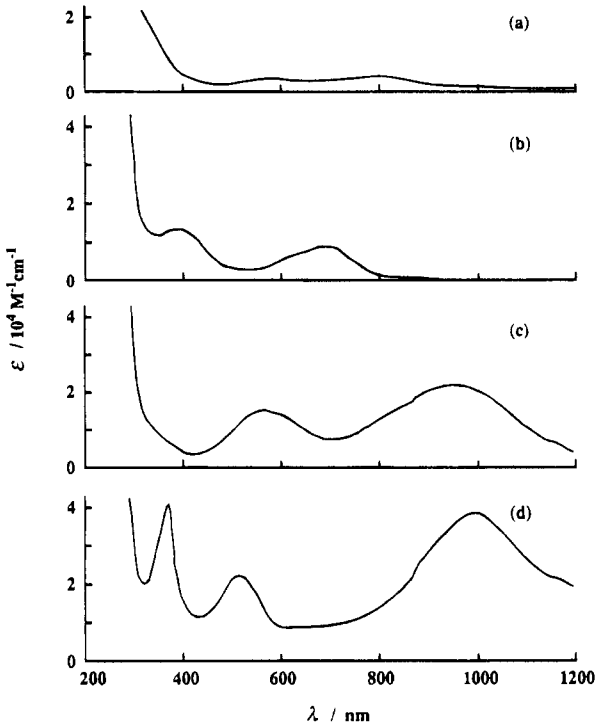

Figure 5. Controlled-potential absorption spectra of $[Ru_3(\mu_3\text{-}O)(\mu\text{-}CH_3CO_2)_6(mbpy^+)_3]^{4+}$ in a 0.1 M $[(n\text{-}C_4H_9)_4N]PF_6$–$CH_3CN$ solution at several applied potentials vs Fc/Fc^+): (a) +0.9 V; (b) no potential applied; (c) −1.0 V; (d) −1.5 V.

examples are dinuclear Ru/Os complexes with π-aromatic polydentate ligands, which show multistep redox waves due to both metal ions and ligands.[1-3] Krejčík and Vlček reported a total of 14 almost reversible one-electron redox waves of $[\{Ru(bpy)_2\}_2(\mu\text{-bpm})](PF_6)_4$ (bpm = 2,2′-bipyrimidine) in DMF at low temperature (−75 °C), consisting of Ru-based (2e) and bpy- and bpm-based (12e) processes;[2] reversibility of some processes in the negative region, however, is lower at room temperature. Versatile electrochemical and spectroscopic properties of a series of polynuclear Ru/Os complexes using polydentate heteroaromatic ligands have also been reported by Balzani *et al.*[4] The system involves more than two redox-active metal centers and redox-active ligands in one molecule, and their redox potentials are tunable by modifying both metal ions and ligands involved. Multistep redox properties in these systems are rather complicated, and their wave assignments sometimes seem to remain obscure. In this context, each redox wave observed in our system is clearly assignable, and furthermore, as stated in the Introduction, their redox potentials can also be controlled by changing metal ions, the bridging carboxylate and the terminal ligands in the trinuclear framework.

The present oxo-centered Ru_3 and the mixed-metal Ru_2Rh complexes with three $mbpy^+$ ligands $[M_3(\mu_3\text{-}O)(\mu\text{-}CH_3CO_2)_6(mbpy^+)_3]^{4+}$ exhibit reversible multistep and multielectron redox behavior. Excellent electrochemical reversibility of several steps involved in these complexes is particularly noted. The present complexes appear to provide one of the most remarkable reversible electron pool systems. The Ru_3 complex provides reversible eight redox steps (I, II, III, IVa, IVb, V, VIa, and VIb) and one irreversible step (VII) which involve a total of 11 electrons in the range from +2.0 to −3.0 V vs Fc/Fc^+ (Figure 2). In the Ru_2Rh complex, six reversible steps (I, II, III, and IVa–IVc) and two irreversible steps (V and VI) which involve a total of 10 electrons are observed in the same potential range (Figure 3). Comparison of redox potential data of trinuclear $mbpy^+$ complexes with those of the corresponding pyridine complexes $[M_3(\mu_3\text{-}O)(\mu\text{-}CH_3CO_2)_6(py)_3]^+$ (M_3 = Ru_3, Ru_2Rh, and Rh_3),[41,51] $[Ru_3(\mu_3\text{-}O)(\mu\text{-}C_6H_5CO_2)_6(py)_3]^+$ [26] and the free ligand $[mbpy^+]PF_6$[46] enables us to assign each redox wave. Further evidence for the ligand-based process ($mbpy^+/mbpy^•$) in Ru_3 complex **2** is obtained by spectroelectrochemical observation of a strong absorption with the band maxima at 370 nm (ϵ = 41 700 M^{-1} cm^{-1}) assignable to a π–π^* transition in coordinated $mbpy^•$ ligands at the potential between processes IVb and V (at −1.5 V). It is observed that the potentials of processes I, II, and III for the trinuclear core-based processes for Ru_3 complex **2** shift to the more positive direction (by 50–130 mV) and that the most negative potential for process VII shifts to the more negative direction (by 310 mV) compared to that for the corresponding processes for the pyridine analog. This trend is also seen in complexes **3** and **4**. The overall complex charge seems to have an important role in determining the redox potentials of the $mbpy^+$ analogs.

Ligand–Ligand Interactions through the Trinuclear Core. In contrast to the extensive studies of ligand–ligand interactions through a mononuclear metal center (e.g. $[Ru(bpy)_3]^{2+}$),[53] those through a cluster core have been scarcely explored.

Ligand-based redox waves ($mbpy^+/mbpy^•$ and $mbpy^•/mbpy^-$) are highly dependent on the metal ions involved in the trinuclear unit. Although the ligand-based process ($mbpy^+/mbpy^•$) does

(53) Multistep ligand-reduction processes in $[Ru(bpy)_3]^{2+}$, see for example: (a) Ohsawa, Y.; DeArmond, M. K.; Hanck, K. W.; Morris, D. E.; Whitten, D. G.; Neveux, P. E., Jr. *J. Am. Chem. Soc.* **1983**, *105*, 6522–6524. (b) Juris, A.; Balzani, V.; Barigelletti, F.; Campagna, S.; Belser, P.; von Zelewsky, A. *Coord. Chem. Rev.* **1988**, *84*, 85–277. (c) Ghosh, B. K.; Chakravorty, A. *Coord. Chem. Rev.* **1989**, *95*, 239–294.

not split in the Rh_3 complex, it splits into two steps with 2:1 current intensity ratio in the Ru_3 complex and three in the mixed-metal Ru_2Rh complex. The splitting between processes IVa and IVb in Ru_3 complexes **2** and **3** is 140 and 110 mV, respectively (Table 3). The splitting pattern of Ru_2Rh complex **4** is accounted for by considering not only different metal centers (Ru and Rh) but also the interaction between the two $mbpy^+$ ligands at the two Ru sites. Although unambiguous assignment of each redox potential is not possible, reductions of two $mbpy^+$ ligands coordinated to the Ru centers in complex **4** occur with at least 120 mV separation (IVa and IVb). These values apparently exceed the calculated statistical potential difference in noninteracting redox-active centers.[54]

Splitting of ligand-reduction processes in metal complexes is generally considered to occur due to the following two factors as pointed out by Vlček:[55] electrostatic repulsions between ligands and metal-mediated ligand−ligand electronic interactions. One-step reductions of three terminal $mbpy^+$ ligands in Rh_3 complex **5** (Figure 4) shows that no electrostatic repulsions exist in this complex. Virtually no electrostatic contribution to the ligand-reduction process(es) is also expected for the Ru_3 and the Ru_2Rh complexes, since they have the identical trinuclear core structures such as bond length and bond angles to those for Rh_3 complexes.[56] This conclusion is further supported by two closely spaced one-electron reductions of $mbpy^+$ ligands in *cis*-$[(bpy)_2Ru(mbpy^+)_2](PF_6)_4$,[45c] in which two $mbpy^+$ ligands are connected by a mononuclear Ru^{II} center. These results allow us to conclude that the splitting observed in the present systems is due to electronic interactions between ligands through the trinuclear core.

Substantial difference in the ligand redox patterns for the Ru_3, the Ru_2Rh, and the Rh_3 complexes seems to be highly relevant to the number of electrons involved in the trinuclear core. It is evident that the $mbpy^+$ reductions occur in the oxidation state of $Ru^{II}Ru^{III}_2$, $Ru^{II}Ru^{III}Rh^{III}$, and Rh^{III}_3 which involve 18, 19, and 20 electrons in the $d\pi-p\pi$ molecular orbitals, respectively. While the molecular orbitals for the Rh^{III}_3 complex are fully occupied with electrons, those for the $Ru^{II}Ru^{III}_2$ and $Ru^{II}Ru^{III}Rh^{III}$ cores have a vacant and a half-filled antibonding orbital, respectively. This antibonding orbital (d_{yz} character) overlaps with π^* orbitals of $mbpy^+$ ligands when the aromatic rings are planar to the $M_3(\mu_3\text{-O})$ plane and may play an important role in mediating interactions between ligands. The vacant (or half-filled) molecular orbital in the trinuclear core seems to have the electronic transmitting properties. This consideration can be further applied to the $mbpy^{\bullet}/mbpy^-$ process for the Ru_3 and the Ru_2Rh complexes: a two-step split character for the Ru_3 complexes **2** and **3** (19-electron $Ru^{II}_2Ru^{III}$ core with the half-filled orbital) and a one-step process for the Ru_2Rh complex **4** (20-electron $Ru^{II}_2Rh^{III}$ core with the fully occupied orbital). Larger separarion in the ligand-reduction processes ($mbpy^+/mbpy^{\bullet}$) in the Ru_2Rh complex compared with the Ru_3 complex shows stronger electronic transmitting properties of the $Ru^{II}Ru^{III}Rh^{III}$ framework. It has been suggested that the Ru−O−Ru unit in the mixed-metal Ru_2Rh complex is electronically localized[41] and is expected to show stronger electronic interactions between the two Ru centers. This also allows stronger electronic interactions between the terminal ligands in the Ru_2Rh complex compared to the Ru_3 complex.

Conclusion

The oxo-centered carboxylate-bridged trinuclear Ru_3 and Ru_2Rh complexes having redox-active $mbpy^+$ ligands exhibit well-defined reversible multistep and multielectron redox behavior in CH_3CN. The complexes would offer a new class of reversible multistep and multielectron redox systems. The patterns of ligand-based waves ($mbpy^+/mbpy^{\bullet}$ and $mbpy^{\bullet}/mbpy^-$) depend on the kinds of metal ions (Ru_3, Ru_2Rh, and Rh_3) and the number of electrons in $d\pi-p\pi$ molecular orbitals in the trinuclear assemblies.

Acknowledgment. This work was supported by Grant-in-Aids for Scientific Research No. 03231105 (Y.S.), Nos. 03241106, 03555184, and 06226102 (S.Y.), and Nos. 02303006, 04453041, and 04241104 (T.I.) from the Ministry of Education, Science and Culture, Japan. S.Y. would like to thank the Nihonitagarasu Foundation and the Iwatani Naoji Foundation for financial support. We also thank Japan Analytical Industry Co. Ltd. for the preparative liquid chromatography, Professor I. Taniguchi and Dr. M. Tominaga (Kumamoto Univ.) for the spectroelectrochemical measurements, and Dr. K. Unoura (Yamagata Univ.) for coulometry.

IC9504957

(54) The potential separations between the first and the nth redox potentials ($\Delta E_{1,n}$) with identical, noninteracting redox centers are expressed by $\Delta E_{1,n} = (2RT/F) \ln n$, where R = gas constant, T = temperature, and F = Faraday constant. This yields $\Delta E_{1,2} = 36$ mV and $\Delta E_{1,3} = 56$ mV at 298 K.: Flanagan, J. B.; Margel, S.; Bard, A. J.; Anson, F. C. *J. Am. Chem. Soc.* **1978**, *100*, 4248−4253.

(55) Vlček, A. A. *Coord. Chem. Rev.* **1982**, *42*, 39−62.

(56) The trinuclear core structures of the Ru_3[19a,26−28] and Rh_3[12a] complexes are quite similar in the solid-state. Almost identical structures of the mixed-metal trinuclear complexes $[Ru_2M(\mu_3\text{-O})(\mu\text{-}CH_3CO_2)_6(py)_3]$ (M = Ni^{II} and Co^{II}) to those of Ru_3 complexes have been also reported.[42a]